References

AUROUX, A., DESEPERT, H., LECLERCQ, C. & VEDRINE, J. (1983). *Appl. Catal.* **6**, 95-119.

BAERLOCHER, C. (1984). Proc. 6th Int. Zeolite Conf., Reno, edited by D. OLSON & A. BISIO, pp. 823-833. Guildford: Butterworths.

BALLMOOS, R. VON (1981). Thesis, Zürich. Frankfurt am Main: Verlag GmbH.

BONDI, A. (1964). *J. Phys. Chem.* **68**, 441-451.

CHAO, K. J., LIN, J. C., WANG, Y. & LEE, G. H. (1986). *Zeolites*, **6**, 35-38.

CROMER, D. T. & MANN, J. B. (1968). *Acta Cryst.* A**24**, 321-324.

FLANIGEN, E. M., BENNETT, J. M., GROSE, R. W., COHEN, J. P., PATTON, R. L., KIRCHNER, R. L. & SMITH, J. V. (1978). *Nature (London)*, **271**, 512-516.

GILSON, J. P. & DEROUANE, E. G. (1984). *J. Catal.* **88**, 538-541.

HAAG, W. O., LAGO, R. M. & WEISZ, P. B. (1984). *Nature (London)*, **309**, 589-591.

JANSEN, J. C., VAN KONINGSVELD, H., SCHALKOORD, D. & VAN BEKKUM, H. (1987). *Zeolites*. To be submitted.

KEIJSPER, J., MACKAY, M., VAN DEN BERG, K., KORTBEEK, A. G. T. G. & POST, M. F. M. (1986). KNCV Katalyse Symposium (Catalysis Symp. of the Royal Dutch Chem. Soc.), 17-18 April, TH Twente, The Netherlands, p. 39.

LERMER, H., DRAEGER, M., STEFFEN, J. & UNGER, K. K. (1985). *Zeolites*, **5**, 131-134.

OLSON, D. H., HAAG, W. O. & LAGO, R. M. (1980). *J. Catal.* **61**, 390-396.

OLSON, D. H., KOKOTAILO, G. T., LAWTON, S. L. & MEIER, W. M. (1981). *J. Phys. Chem.* **85**, 2238-2243.

PRICE, G. D., PLUTH, J. J., SMITH, J. V., BENNETT, J. M. & PATTON, R. L. (1982). *J. Am. Chem. Soc.* **104**, 5971-5977.

SHELDRICK, G. M. (1976). *SHELX*76. Program for crystal structure determination. Univ. of Cambridge, England.

SPEK, A. L. (1982). The *EUCLID* package. In *Computational Crystallography*, edited by D. SAYRE, p. 528. Oxford: Clarendon Press.

STEWART, J. M., KRUGER, G. J., AMMON, H. L., DICKINSON, C. W. & HALL, S. R. (1972). The *XRAY*72 system. Tech. Rep. TR-192. Computer Science Center, Univ. of Maryland, College Park, Maryland.

ZALKIN, A. (1957). *Acta Cryst.* **10**, 557-560.

Acta Cryst. (1987). B**43**, 132-143

Conflicting Results for the Deformation Properties of Forsterite, Mg_2SiO_4

BY ROB J. VAN DER WAL AND AAFJE VOS

Department of Chemical Physics, University of Groningen, Nijenburgh 16, 9747 *AG Groningen, The Netherlands*

AND ARMIN KIRFEL

Mineralogisches Institut der Universität Bonn, Lehrstuhl für Mineralogie und Kristallographie, Poppelsdorfer Schloss, D-5300 *Bonn* 1, *Federal Republic of Germany*

(*Received* 18 *July* 1985; *accepted* 21 *August* 1986)

Abstract

Deformation properties of forsterite have been deduced simultaneously from X-ray diffraction data affected by extinction in Bonn-Pittsburgh (*B*), and in Groningen (*G*). For the *G* crystals, *G*I and *G*II, extinction is anisotropic and considerably larger than for crystal *B*. Measurements were made with Mo radiation for *B*, and with Mo and Ag radiation for *G*I and *G*II. As the Becker & Coppens [*Acta Cryst.* (1974), A**30**, 129-147, 148-153; *Acta Cryst.* (1975), A**31**, 417-425] extinction model is not exact, the deformation properties had to be filtered from the data with refinement models. The flexible *B* model [α's and populations for single exponential functions (SEF's) refined for $l = 0$-4] and the more rigid *G* model (SEF populations refined for $l = 0$-3 and α for $l = 0$; further α's and n's fixed at standard values) yield different results. Refinement of α makes the majority of the SEF's notably diffuse, presumably due to correlation with incorrect extinction corrections. The order of the deformation potentials at the Mg(1) and Mg(2) sites is reversed for *B* and *G*. Maxima on the Si–O bonds, which are polarized towards O, are smaller for *G* (0·20–0·25 e Å^{-3}) than for *B* (0·25–0·45 e Å^{-3}). Although each of the two sets of deformation properties looks acceptable by itself, the present comparison shows that neither of them may be sufficiently close to the truth. The diffraction data are available on request from the Electron Density Data Bank (Professor H. Burzlaff, Institut für Angewandte Physik, Bismarckstrasse 10, D-8520 Erlangen, Federal Republic of Germany). Details of the measurements are described in the paper.

Introduction

The present paper describes two independent attempts, in Bonn-Pittsburgh (*B*) and in Groningen (*G*), to determine the deformation properties of forsterite by X-ray diffraction. The conflicting results obtained show that incorrect conclusions can be drawn from deformation densities and potentials which, judged by themselves, seem reliable.

0108-7681/87/020132-12$01.50

Forsterite belongs to the group of olivines with composition M_2SiO_4(M = Mg, Fe, Mn, Ca, Cr). For the present work synthetic forsterite with composition Mg_2SiO_4 has been used. The orthorhombic forsterite structure (space group No. 62, *Pbnm*, $Z = 4$) has been described in the literature (Birle, Gibbs, Moore & Smith, 1968). Projections of the structure are shown in Fig. 1. The following features are of interest for this work: (1) The presence of two independent Mg atoms, Mg(1) lying on an inversion center and Mg(2) lying on a mirror plane. It is important to know whether differences exist between the electrostatic properties in the voids containing the Mg atoms. (2) Along the x direction successive O_4 tetrahedra share alternately corners and faces (Fig. 1*b*). The atoms O(−1), Si and O(2) of the independent SiO_4 tetrahedron lie on a mirror plane, O(3) and O(3^{ii}) are related by this plane. The tetrahedron contains pseudo-threefold symmetry around Si–O(−1) and is elongated along **a**. The edges in the base plane O(2)–O(3)–O(3^{ii}) with average length 2·57 (2) Å are considerably shorter than the edges between the base-plane O atoms and the apex O(−1), which average to 2·76 (2) Å (Table 8). The distances Si–O(−1) = 1·6141(2), Si–O(2) = 1·6561 (1) and Si–O(3) = 1·6378 (1) Å show that Si is displaced towards the apex. A study of deformation densities obtained by X-ray diffraction may give information on possible bonding differences between the Si–O (apex) and Si–O (base plane) bonds.

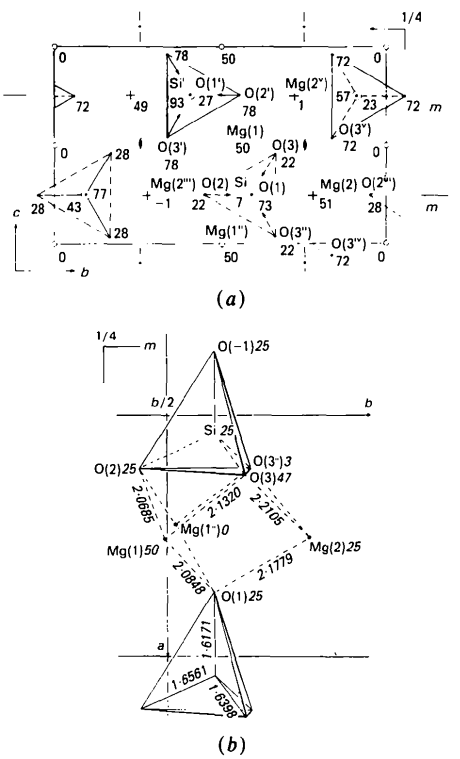

Fig. 1. Projections of the forsterite structure along (*a*) [100] and (*b*) [001] with numbering and heights of the atoms (in units of 0·01*a*) and symmetry elements. The atoms Si, Mg(1), Mg(2), O(1), O(2) and O(3) correspond with the coordinates of Table 7. $A(-1)$ lies one translation period along **a** lower than $A(1)$, and $A(+1)$ one period higher. ○ = Mg(1), + = Mg(2), ⊙ = superposition of Si and O(1), • = O. The SiO_4 tetrahedra are shown schematically. Edges of the base plane, at $x - 0{\cdot}25$ are given by dashed lines, and those at $x - 0{\cdot}75$ by full lines. The O (base plane) - - - O(apex) lines are dashed for tetrahedra pointing down, and drawn in full for tetrahedra pointing up. The latter lines terminate in an arrow if the apex is not at the height given in the figure, but shifted by ±**a**.

Table 1. *Cell dimensions measured for forsterite*

	Bonn	Groningen
Crystal	*B*	*G*II
Diffractometer	Syntex $P2_1$	Nonius CAD-4
Radiation	Mo $K\bar{\alpha}$, λ = 0·71069 Å	Mo $K\alpha_1$, λ = 0·70926 Å
Monochromator	Graphite, 2θ = 12.2°*	
Reflections	25 independent $2\theta > 30°$	22 independent $2\theta > 141°$†
a (Å)	4·757 (1)	4·7550 (3)
b	10·197 (1)	10·1960 (6)
c	5·982 (1)	5·9809 (3)
V (Å^3)	290·17 (14)	289·97 (5)

* For *G*II with beam flattener described by Helmholdt & Vos (1977).
† Determined by J. L. de Boer with α_1 radiation only.

Crystal data

Crystal samples, cell dimensions

Three spherical crystals have been used for the data collection. One crystal (*B*) with diameter ∅ = 0·200 (6) mm in Bonn and two crystals, *G*I with ∅ = 0·42 (1) and *G*II with ∅ = 0·20 (1) mm, in Groningen. The *B* and *G* cell dimensions presented in Table 1 agree within experimental error.

Quality of the samples

The Bonn crystal was ground from a single-crystal fragment of synthetic forsterite containing negligible traces of Mn and Fe, and about 0·013 wt% Cr^{3+}. This sample, originally grown by the Czochralsky method (Union Carbide), was kindly provided by S. Hafner (University of Marburg, Federal Republic of Germany). In order to reduce extinction effects the sample was dipped a few times into liquid nitrogen during the grinding procedure. A final check for the crystal quality was made by Weissenberg photographs.

The *G* crystals were ground from a sample kindly provided by G. V. Gibbs (Virginia Polytechnic Institute and State University, Blacksburg, VA). The sample was synthesized by reaction of stoichiometric mixtures of SiO_2 and MgO in the presence of H_2O at temperatures above 770 K and pressures between 135 and 675 atm (1 atm = 0·1013 MPa). Single crystals were prepared by the Verneuil (flame fusion) technique. The samples were chemically pure and homogeneous within the analytical error of the electron microprobe. Spectroscopic analysis indicated trace amounts of Al and Cu of less than 200 p.p.m.

Table 2. *Data collection for B, GI and GII*

	B	*GI*, Mo	*GI*, Ag	*GII*, Mo	*GII*, Ag
Crystal diameter (mm)	0·200 (6)	0·42 (1)		0·20 (1)	
Radiation	Mo $K\alpha$	Mo $K\alpha$	Ag $K\alpha$	Mo $K\alpha$	Ag $K\alpha$
Wavelength (Å)	0·71069	0·71069	0·56083	0·71069	0·56083
Max. (sin θ/λ) (Å^{-1})	1·322	1·31	1·66	1·36	1·02§
Diffractometer	Syntex $P2_1$	CAD-3*		CAD-4F	
Monochromatization	Graphite monochromator	Zr filter	Pd filter	Graphite monochromator†	
Tube voltage (kV)	50	50	50	50	40
Normal amps (mA)	20	35	35	32	32
Amps strong reflections		3·5	3·5	3·2	3·2
Mosaic spread (°)		0·5		0·4	
Scan mode	θ–2θ	θ–2θ	θ–2θ	θ–2θ	θ–2θ
Step scan (number of steps)	Yes (96)	No	No	Yes (96)	Yes (96)
Scan range (°)	$2{\cdot}0+\Delta\lambda(\alpha_1,\alpha_2)$	$0{\cdot}7+0{\cdot}5\tan\theta$	$0{\cdot}7+0{\cdot}67\tan\theta$	$1{\cdot}3+\tan\theta$	$1{\cdot}3+\tan\theta$
Horizontal slit width (°)	2·0	0·88	0·88	1·62	1·62
Vertical opening		1·5	1·5	1·5	1·5
Time ratio T_P/T_B	1·0	2·0	2·0	Profile analysis	
Scan speed (° min^{-1})	1·0–10·0				
Desired $\sigma(I)/I$		0·015	0·015	0·010	0·010
t(max) on reflection (s)	260	150	150	75	75
Number of reference reflections	6 ±(004; 080; 701)	3 (13$\bar{9}$; 014$\bar{1}$; 61$\bar{1}$)	3 (116; 24$\bar{1}$; 24$\bar{2}$)	3 (13$\bar{9}$; 014$\bar{1}$; 61$\bar{1}$)	3 (116; 24$\bar{1}$; 24$\bar{2}$)
Interval‡	28 reflections	3 h	3 h	2 h	2 h
Octants measured	8§	2	1	4	8§
Number of reflections	12 877	6618	6443	18 416	25 356
Multiple reflection check	No	No	No	Yes	Yes¶
Number of unique reflections**	1752	5325	5826	10 453	7707
Number with $I<3\sigma(I)$	223	255	1442	1068	2652
Internal match	0·03††				0·01††

* Measured by J. L. de Boer.
† With beam flattener (Helmholdt & Vos, 1977). Al wire, $\varnothing = 0{\cdot}55$ mm, $\Delta I = 1{\cdot}5\%$ over 0·5 mm.
‡ For *B* and *GII* complete set of reference reflections measured, for *GI* only one reflection.
§ *B*: $2\theta > 100°$ weak reflections omitted (see text). *GII*(Ag): one octant up to sin $\theta/\lambda = 1{\cdot}5$ Å^{-1}, reflections counted up to sin $\theta/\lambda = 1{\cdot}02$ Å^{-1}.
¶ According to van der Wal & Vos (1979).
** For *GI* and *GII* symmetry *P*1 because of extinction.
†† Defined in the text.

All three crystals were washed with dilute hydrofluoric acid to remove flakes from the crystal surfaces.

Determination of $|F(hkl)|$

Data collection and reduction

Details of the measurements and data reduction are given in Table 2 and below.† Intensities were collected on diffractometers. For *B* only Mo radiation was applied, for *GI* and *GII* both Mo and Ag radiations. Individual intensities have been adjusted to (average) changes in reference intensities and have been corrected for Lorentz and polarization effects. Absorption corrections were made for the *GI* and *GII* data according to the formula

$$I(\text{corr}) = A^* I(\text{obs}), \qquad (1a)$$

with A^* given by *International Tables for X-ray Crystallography* (1972)

$$A^*(GI;\text{Mo}) = 1{\cdot}390\,(1-0{\cdot}01191\theta);$$
$$A^*(GI;\text{Ag}) = 1{\cdot}189\,(1-0{\cdot}00321\theta) \qquad (1b)$$
$$A^*(GII;\text{Mo}) = 1{\cdot}171\,(1-0{\cdot}00318\theta);$$
$$A^*(GII;\text{Ag}) = 1{\cdot}086\,(1-0{\cdot}00064\theta). \qquad (1c)$$

The glancing angle θ is in radians. For individual G intensities the maximum difference $\Delta A^*_{\max}/A^*$ varies from 0·04 to 1·4% for the different data sets. For crystal *B* $\Delta A^*_{\max}/A^* = 0{\cdot}4\%$ was considered to be small in comparison with other systematic errors, and no corrections for absorption were applied.

In contrast to crystal *B*, crystals *GI* and *GII* show considerable intensity differences between equivalent reflections (up to 15% for the Mo data of *GII*). As this indicates the presence of anisotropic extinction, only intensities of reflections **H** and **−H** could be averaged.

Details for crystal B

During the first four months of the intensity measurements the sums of the standard intensities showed a steady decrease of about 16%, whereas after levelling off fluctuations in the order of 1% occurred. Up to a maximum $2\theta = 100°$ all reflections in reciprocal space have been measured. Between $100 < 2\theta \leq 140°$ data collection has been restricted to reflections which were expected to be observable on the basis of F(calc) calculations after preliminary refinement with the data up to $2\theta = 100°$. The internal match for the complete data set given in Table 2 corresponds with the (unweighted) consistency factor

$$R_{\text{int}} = \sum_{\mathbf{H}}\sum_{i} |I(\mathbf{H}) - I(\mathbf{H},i)| \Big/ \sum_{\mathbf{H}}\sum_{i} I(\mathbf{H},i). \qquad (2)$$

The summation **H** is over the unique reflections and i refers to all reflections within a symmetrically related

† Lists of structure factors for *B* (Mo), *GI* (Mo and Ag) and *GII* (Mo and Ag) have been deposited with the British Library Document Supply Centre as Supplementary Publication No. SUP 43277 (140 pp.). Copies may be obtained through The Executive Secretary, International Union of Crystallography, 5 Abbey Square, Chester CH1 2HU, England.

set. The standard deviations $\sigma_c(\mathbf{H}; |F|)$ in the average F values are based on counting statistics alone and may therefore be somewhat underestimated.

Details for crystals GI and GII

During the intensity measurements for *GI* on the CAD-3 the reference intensities decreased gradually by 3·5% for both radiations. For the *GII* measurements on the CAD-4F both radiations showed a gradual decrease in reference intensities from 100 to 80% during the long-lasting data collection (8 months for Mo and 4 months for Ag). Moreover, there turned out to be more or less random fluctuations of 1·5%. Repeated measurements of the reflection 116 with a statistical accuracy $\sigma(I)/I = 0{\cdot}1\%$ showed occasional discrepancies up to 2%. Analysis of the reflection profiles indicated that these variations could be ascribed to irregularities in the motor speed. The uncertainties are larger than errors due to counting statistics, but may partly be balanced by the availability of symmetrically equivalent reflections from different octants. The CAD-4F profiles were analyzed according to method I in van der Wal, de Boer & Vos (1979) with special precautions for overlapping reflection profiles; $B = 1{\cdot}03$, $A(\text{Mo}) = 0{\cdot}37\,(8)°$, $A(\text{Ag}) = 1{\cdot}10\,(3)°$, $SM = 2{\cdot}7$, $TH = 0{\cdot}2$.

Normal and reduced-current reflections were put on the same relative scale by the procedure of Hamilton, Rollett & Sparks (1965) with use of reflections measured in both ways. Weights $w_c(\mathbf{H}; I)$ based on counting statistics were applied. For the (*GII*; Ag) set 12 pairs of reflections with $|I(\mathbf{H}) - I(-\mathbf{H})| > 10{\cdot}0 \times [w_c(\mathbf{H}; I) + w_c(-\mathbf{H}; I)]^{-1/2}$ were removed from the list. For the remaining Friedel-related reflections $\mathbf{H}$ and $-\mathbf{H}$ the internal match given in Table 2 corresponds with the weighted consistency factor:

$$R_w(I; \mathbf{H}, -\mathbf{H}) = \left[\sum_{\mathbf{H}} w_c(\mathbf{H}; I)|I(\mathbf{H}) - \overline{I(\mathbf{H}, -\mathbf{H})}|^2 \Big/ \sum_{\mathbf{H}} w_c(\mathbf{H}; I)|I(\mathbf{H})|^2\right]^{1/2}, \quad (3)$$

where $\mathbf{H}$ runs over all individual reflections. For each data set weighted average intensities $\overline{I(\mathbf{H})}$ were calculated from the values $I(\mathbf{H})$ and $I(-\mathbf{H})$, which in some cases were measured more than once because of the scaling. Finally, for both crystals weak high-order reflections were used to determine a preliminary scale factor between the Mo and Ag data.

Structure refinements and results

Multipole refinements; comparison of B and G models

Full-angle multipole refinements have been carried out for both the *B* and *G* crystals. Details are given in Table 3. For *B* the multipole refinements were preceded by full-angle and high-angle (HO) conventional refinements (see below).

In the program *VALRAY* (Stewart, 1976; Stewart & Spackman, 1981) the density of each pseudo-atom p, with respect to its nucleus as origin, is written as

$$\rho_p(\mathbf{r}_p) = \text{Pop}_p^{\text{sph}} \rho_p^{\text{sph}}(r_p) + \Delta\rho_p(\mathbf{r}_p) \quad (4a)$$

with

$$\Delta\rho_p(\mathbf{r}_p) = \sum_l \sum_{m=0}^{l} \left[\sum_i \text{Pop}_p(l, m, i)\rho_p(l, i; r_p)\right] Y_{lm\pm}(\theta, \varphi), \quad (4b)$$

r_p, θ and φ being the polar coordinates of $\mathbf{r}_p$. $Y_{lm\pm}(\theta, \varphi)$ are Tesseral harmonics and $\rho_p^{\text{sph}}(r_p)$ is the unperturbed density of atom p, normalized to one electron. $\rho_p^{\text{sph}}(r_p)$ is represented by Hartree-Fock (HF) scattering factors, and the radial distributions of the deformation functions are described by single exponential functions (SEF's):

$$\rho_p(l; r_p) = N_{n,l}\, r_p^n \exp(-\alpha_{p,l} r_p) \text{ with } n \geq 1 \quad (5)$$

with

$$N_{n,l} = (1/4\pi)\alpha^{n+l+3}/(n+l+3)! \quad (5a)$$

The pseudo-atoms are considered as rigid, which implies that for each atom p the thermal motion is taken the same for all terms in (4).

The applied models show the following differences:

(1) α's are refined for *B* and, apart from monopole α's, are taken constant for *G*. For *B* divergence was avoided by alternate refinement of independent-atom and deformation parameters, and by damping of the parameter shifts. For *G* the constant α values have the disadvantage of making the *G* model rigid. Moreover, it is not *a priori* known which α's should be taken. For instance, fitting SEF's to the [2, 2] theoretical scattering curve for diatomic Si–O [van der Wal, Vos & Stewart (1987); two terms used for monopoles; for $l = 0$ generally accepted values adopted for n] gives radial distribution functions which tend to be more diffuse than the distributions adopted for the *G* refinement (Table 4). In particular, the *G* refinement dipoles and quadrupoles are too sharp in comparison with the corresponding Si–O functions. On the other hand, inclusion of both α's and extinction parameters in the refinement as performed for *B* may yield radial distribution functions which are too diffuse (Stewart, 1985). Table 5 shows that the refined α values for *B* are in general considerably smaller than the standard molecular values. Even in comparison with the Si–O model, dipole and quadrupole deformations at Si and octapole deformations at O are far too diffuse (Table 4). The tendency of the deformation functions to become too diffuse, when refined, indicates that the refinement yields multipole parameters which, in combination with extinction, can adjust $Y^{1/2}(\mathbf{H})F_c(\mathbf{H})$ to $F_o(\mathbf{H})$ in the low-order region.

Table 3. *Details for the final stages of the multipole refinements*

	Crystal *B*	Crystal *GI*	Crystal *GII*
Least-squares Q function	$Q=\sum_{\mathbf{H}} w(F;\text{Mo})[F_o(\text{Mo};\mathbf{H})-F_c(\mathbf{H})\,Y^{1/2}(\text{Mo};\mathbf{H})]^2$	$Q=\sum_{\mathbf{H}} w(F;\text{Mo})[F_o(\text{Mo};\mathbf{H})-F_c(\mathbf{H})\,Y^{1/2}(\text{Mo};\mathbf{H})]^2$ $+\sum_{\mathbf{H}} w(F;\text{Ag})[F_o(\text{Ag};\mathbf{H})$ $-k'F_c(\mathbf{H})\,Y^{1/2}(\text{Ag};\mathbf{H})\exp(-8\pi^2\Delta U\sin^2\theta/\lambda)^2]^2$	
F weights	$w=[\sigma^2_{\text{count}}(\lvert F_o\rvert)]^{-1}$	$w=[\sigma^2_{\text{count}}(\lvert F_o\rvert)]^{-1}$	$w=1{\cdot}0$*
f^{sph}	Clementi (1965) SCF (Mg^{2+}, Si, O)	Clementi (1965) SCF (neutral atoms)	
Anomalous dispersion	Cromer & Liberman (1970)	Cromer & Liberman (1970)	
Extinction	Isotropic type 1, Becker & Coppens, Lorentzian mosaic spread	General Becker & Coppens formalism, Gaussian mosaic spread according to Nelmes (1980)	
Deformation functions	SEF of type $r^n\exp(-\alpha r)$ normalized to 1 electron for $l=0$; two monopoles per atom	SEF of type $r^n\exp(-\alpha r)$ normalized to 1 electron for $l=0$; one monopole per atom	
l values (i for $l=0$)	O(1) O(2) 1 2 3 4	O(1) 1 2 3	
Constraints			
Si n	3 4 4 4 4 4	4 4 4 4	
α	3·50‡	3·50 3·50 3·50	
Mg n	3 4 4 4 4 4	4 4 4 4	
α†	3·00‡	3·00 3·00 3·00	
O n	2 3 2 2 3 4	4 2 2 2	
α	4·50‡	4·50 4·50 4·50	
Pop's	Pop(sph; Si):Pop(sph; Mg^{2+}):Pop(sph; O) = 14:10:8 Pop(sph; Mg2) = Pop(sph; Mg1) Pop(0,0,2; Mg2) = Pop(0, 0, 2; Mg1) Pop(sph; O1) = Pop(sph; O2) = Pop(sph; O3) Pop(0,0,1; O1) = Pop(0,0,1; O2) = Pop(0,0,1; O3)	Pop(sph; Si):Pop(sph; Mg):Pop(sph; O) = 14:12:8 $\sum_p \text{Pop}_p(0,0,1)=0$	
U		$\Delta U(\text{Ag})\equiv 0$	$\Delta U(\text{Ag})=71\,(9)\times10^{-5}$ Å^2§
N	1516	10 186	18 227
N_v	171	121	122
wR	0·012	0·021	0·034

* $w=0$ for 1281 inaccurately measured high-order reflections.
† $\alpha(\text{Mg1})=\alpha(\text{Mg2})$.
‡ $\alpha=2\xi$ (Hehre, Stewart & Pople, 1969).
§ $\Delta U(\text{Ag})$ accounts for additional decrease of Ag intensities with $\sin\theta/\lambda$, presumably due to systematic measuring errors.

Table 4. *Comparison of B and GII SEF's with theoretical SEF's for* SiO (*see text*)

r_m (Å) is the r_p value for which SEF is maximal. For B α's of O atoms are averaged.

	$l=0$			$l=1$			$l=2$			$l=3$			$l=4$		
Si	n	α	r_m	n	α	r_m	n	α	r_m	n	α	r_m	n	α	r_m
SiO(SEF)	3·24*	2·30*	0·75	4	2·96	0·72	4	2·83	0·75						
B	4	4·0†	0·53	4	1·4	1·51	4	1·4	1·51	4	2·4	0·88	4	2·2	0·96
G	4	3·02	0·70	4	3·5	0·60	4	3·5	0·60	4	3·5	0·60			
SiO(SEF)	3·07*	2·95*	0·55	2	2·00	0·53	2	3·37	0·31						
B	3	2·9	0·55	2	1·8	0·59	2	2·0	0·53	3	1·9	0·84	4	1·9	1·11
G	4	3·76	0·56	2	4·5	0·24	2	4·5	0·24	3	4·5	0·35			

* Average of two terms weighted according to populations. SEF of first term fixed with for Si $n=4$, $\alpha=3{\cdot}5$ and for O $n=2$, $\alpha=4{\cdot}5$. For the second term $n=3$ for both Si and O.
† Refined $\alpha=3{\cdot}97$ (5) for $n=4$, added to fixed monopole with $n=3$ and $\alpha=3{\cdot}50$.

Table 5. *Averaged refined values for crystal B*

l	0	1	2	3	4	2ξ*
Si	4·0	1·4	1·4	2·4	2·2	3·5
Mg	4·6	3·1	1·9	2·7	1·8	3·0
O	2·9	1·8	2·0	1·9	1·9	4·5

* Hehre, Stewart & Pople (1969).

This implies that the electron density distribution filtered from the $F_o(\mathbf{H})$ values is not unique, but affected by the set-up of the multiple refinement and by systematic errors in the $F_o(\mathbf{H})$ values which are not accounted for by the applied extinction correction.

(2) *B* multipoles extend to higher orders (up to hexadecapoles) than *G* multipoles (up to octapoles). The *B* hexadecapoles are again rather diffuse (Table 4), but have at least two populations exceeding 3σ for each of the atoms.

(3) There are different types of constraints between the populations (Table 3). The *G* constraints keep the crystal electroneutral and the estimated scale factor

$$K(\text{multi})=\sum_p \text{Pop}_p^{\text{sph}}(\text{free atom})\Big/\sum_p\sum_i[\text{Pop}_p^{\text{sph}}+\text{Pop}_p(00i)] \quad (6)$$

is transformed into

$$K^G=\text{Pop}_p^{\text{sph}}(\text{free atom})/\text{Pop}_p^{\text{sph}}(\text{multi}). \quad (7)$$

(4) Unequal treatment of Mg atoms. For *B* Mg^{2+} is taken as reference and the constraint $\alpha(l=0;\text{Mg1})=\alpha(l=0;\text{Mg2})$ is used. The *G* reference is

Table 6. *Monopole populations and α's for* Mg(1) *and* Mg(2)

*G*I data omitted since deformation maps for *G*I are not discussed.

	B relative to Mg^{2+}		*G*II* relative to Mg		Gross atomic charges	
	Pop†	α	Pop†	α	*B*	*G*II
Mg(1)	0·20 (14)	4·6 (2)	−1·94 (34)	2·4 (2)	1·80 (14)	1·94 (34)
Mg(2)	0·22 (36)	4·6 (2)	−0·43 (24)	2·9 (7)	1·78 (36)	0·43 (24)

* Correlation coefficients ρ[Pop; α] = 0·80 for Mg(1) and 0·76 for Mg(2). Ratio of SEF coefficients $\text{Pop(Mg1)}\alpha^7\text{(Mg1)}/\text{Pop(Mg2)}\alpha^7\text{(Mg2)} = 1{\cdot}2$.
† After renormalization.

Mg and no constraint for $\alpha(l=0; \text{Mg})$ is applied. Table 6 shows that for *B* the Mg(1) and Mg(2) populations are equal within experimental error; $\sigma[\text{Pop}^B\text{(Mg2)}]$ is relatively large. For *G*II $\alpha(\text{Mg2}) > \alpha(\text{Mg1})$ and $\text{Pop(Mg2)} < \text{Pop(Mg1)}$. The large correlation between Pop and α emphasizes the well known fact that gross atomic charges depend on the shape of the radial distribution functions. This results in large standard deviations, the considerable difference of 1·35 e between the *B* and *G*II gross atomic charges being 3·1 times its e.s.d.

(5) Weights are based on statistical accuracy for *B* and *G*I, and $w = 1$ for *G*II. For the complete hemisphere measured for *G*II, $w = 1$ has the advantage that the refinement converges to (Wilson, 1976)

$$\int [\rho_o(\mathbf{r}) - \rho_c(\mathbf{r})]^2 \, \mathbf{dr} \text{ minimum.} \qquad (8)$$

(6) Isotropic extinction correction for *B* and anisotropic correction for *G*. For *B* correction according to Becker & Coppens (1974), Lorentzian mosaic spread, type 1. For *G* correction according to the general Becker & Coppens (1974, 1975) formalism. Simultaneous use of Mo and Ag data enabled anisotropic refinement of mosaic block size and (Gaussian) mosaic spread.

Details for conventional B refinements

For full-angle refinements extinction corrections are as described above. Scattering factors considered are:

(1) HF scattering factors deduced from Clementi's (1965) wave functions for neutral atoms.

$$R = [\sum |\Delta F|^2 / \sum |F|^2]^{1/2} = 0{\cdot}0233,$$
$$wR = [\sum w|\Delta F|^2 / \sum w|F|^2]^{1/2} = 0{\cdot}0288.$$

Atomic parameters do not change significantly on replacing Mg by Mg^{2+}.

(2) Zeroth-order parts of generalized scattering factors (ZO-GSF's) deduced from accurate wave functions for the diatomics SiO and MgO (McLean & Yoshimine, 1967) and described by multipole expansions up to the [4, 4] and [3, 3] level respectively (Stewart, Bentley & Goodman, 1975; Bentley & Stewart, 1976). The ZO-GSF's represent charged entities $Mg^{1{\cdot}25+}$, $Si^{1{\cdot}32+}$ and $O^{1{\cdot}32-}$. Consequently, the model contained a surplus of 1·46 electrons per formula unit. The indices $R = 0{\cdot}0220$ and $wR = 0{\cdot}0235$ show that, as for $LiBO_2$ (Kirfel, Will & Stewart, 1983), ZO-GSF's are superior to HF scattering factors for conventional full-angle refinements. Scale, coordinates and thermal parameters listed in Table 7 are taken from HO refinements with lower bound $\sin\theta/\lambda = 0{\cdot}8$ Å^{-1}, HF scattering factors, $K^B = 1{\cdot}01(1)K^B$ (multi), $R = 0{\cdot}0207$, $wR = 0{\cdot}0173$.

Coordinates and thermal parameters

Results are listed in Table 7. In general corresponding values show good agreement. Differences *d* between individual coordinates and corresponding weighted average values are $<2{\cdot}5\sigma(d)$ for *G*I, *G*II and *B*(HO), apart from $d[y(\text{O1; GII})] = 2{\cdot}7\sigma(d)$. Largest *d* values, in terms of $\sigma(d)$, for *B*(multi) are $d(x, \text{O2}) = 2{\cdot}6\sigma = 5\times10^{-4}$ Å, $d(x, \text{O3}) = 2{\cdot}7\sigma = 5\times10^{-4}$ Å, $d(y, \text{O3}) = 3.3\sigma = 11\times10^{-4}$ Å, $d(x, \text{O1}) = 5{\cdot}4\sigma = 9\times10^{-4}$ Å.

Differences $>3\sigma$ between corresponding thermal parameters for the *B* and *G* crystals occur only for the multipole values u_{22}(Si) and u_{22}(Mg). Since a similar discrepancy exists between corresponding HO values for *B* and *G*, the difference is not likely to be due to correlation with quadrupole deformation functions. The observed difference, 3×10^{-4} Å^2, causes a difference of only about 3% in the temperature factor at $\sin\theta/\lambda = 1{\cdot}0$ Å^{-1}.

Since the mean coordinates of Table 7 are considered to be the most accurate coordinates available for forsterite, bond lengths and angles based on these coordinates are presented in Table 8.

Extinction

B shows relatively small isotropic extinction with $Y^{1/2}(\text{Mo}) < 0{\cdot}90$ for 16 reflections. The largest deviation of $F_o(\mathbf{H})/Y^{1/2}(\mathbf{H})F_c(\mathbf{H})$ from 1 is observed for reflection 062 (1·03). Extinction is considerable and anisotropic for *G*I and *G*II. Surprisingly, the smallest crystal *G*II exhibits the largest extinction. The smallest $Y^{1/2}$(Mo) values are 0·42 for *G*I and 0·29 for *G*II. For each set of related reflections the average value of $F_o/Y^{1/2}F_c$ is given by

$$\text{Ext}(\mathbf{H}) = \sum\sum [F_o(\mathbf{H}; i, j)/Y^{1/2} \times (\mathbf{H}; i, j)F_c(\mathbf{H}; i, j)]/2n(\mathbf{H}), \qquad (9)$$

where $i = 1$ to $n(\mathbf{H})$ gives the summation over the $n(\mathbf{H})$ symmetrically related reflections, and $j = 1, 2$ stands for Mo or Ag. For *G*II Ext (**H**) deviates most from 1 for the reflections 130 (Ext = 0·97) and 062 (Ext = 1·03). Individual reflections within a set show strong variations in $F_o/Y^{1/2}F_c$, however. An extreme case is the set {222} with $F_o/Y^{1/2}F_c$ ranging from

Table 7. *Positional and thermal parameters: B, GI and GII give results for multiple refinements, and B(HO) for the B high-order refinement*

Positional parameters and u_{ij}(Å^2) are multiplied by 10^5. ΔU(Ag; GII) = 71(9) × 10^{-5}. Mean = weighted average of B(HO), GI and GII. The temperature factor is defined as $T(hkl) = \exp[-2\pi^2(h^2a^{*2}u_{11} + k^2b^{*2}u_{22} + \cdots + 2klb^*c^*u_{23})]$.

		x	y	z	u_{11}	u_{22}	u_{33}	u_{12}	u_{13}	u_{23}	u_{eq}
Si	*B*	7358 (3)	59404 (2)	25000	249 (4)	355 (4)	354 (4)	−6 (4)	0	0	319
	B(HO)	7351 (4)	59404 (3)		244 (6)	363 (5)	357 (5)	2 (5)			321
	GI	7354 (1)	59405 (1)		270 (1)	383 (1)	367 (1)	4 (1)			340
	GII	7356 (2)	59404 (1)		266 (4)	383 (4)	359 (4)	5 (2)			336
	Mean	7354 (1)	59404 (1)								
Mg(1)	*B*	50000	50000	50000	445 (6)	637 (6)	438 (6)	19(5)	−57 (6)	116 (5)	507
	B(HO)				432 (8)	632 (11)	422 (7)	21 (7)	−55 (7)	115 (8)	495
	GI				440 (2)	664 (2)	443 (2)	17 (1)	−53 (1)	107 (1)	516
	GII				437 (5)	664 (6)	432 (5)	14 (3)	−53 (3)	111 (3)	511
Mg(2)	*B*	50840 (5)	77741 (2)	25000	530 (6)	437 (6)	532 (6)	−6 (6)	0	0	500
	B(HO)	50841 (6)	77731 (3)		525 (8)	432 (11)	511 (7)	−17 (7)			489
	GI	50835 (1)	77738 (1)		533 (2)	453 (2)	541 (2)	−18 (1)			509
	GII	50842 (3)	77737 (2)		532 (5)	457 (5)	530 (5)	−16 (3)			506
	Mean	50836 (1)	77737 (1)								
O(1)	*B*	73376 (7)	59154 (4)	25000	297 (12)	629 (15)	544 (13)	−3 (11)	0	0	490
	B(HO)	73395 (10)	59144 (5)		304 (11)	606 (16)	520 (13)	−5 (12)			477
	GI	73414 (3)	59152 (1)		313 (3)	619 (3)	523 (3)	−10 (3)			485
	GII	73422 (6)	59161 (3)		300 (7)	627 (9)	514 (8)	−19 (6)			480
	Mean	73414 (3)	59153 (1)								
O(2)	*B*	22159 (8)	44709 (4)	25000	466 (14)	413 (14)	575 (13)	−16 (11)	0	0	485
	B(HO)	22174 (11)	44715 (5)		469 (13)	395 (11)	584 (13)	−5 (12)			482
	GI	22169 (3)	44706 (1)		475 (3)	382 (3)	568 (3)	−1 (3)			475
	GII	22175 (6)	44701 (3)		460 (8)	392 (8)	562 (8)	−17 (6)			471
	Mean	22170 (3)	44705 (1)								
O(3)	*B*	22283 (7)	66323 (3)	46692 (5)	476 (10)	613 (11)	492 (9)	−27 (7)	−18 (7)	−136 (7)	527
	B(HO)	22272 (8)	66312 (4)	46692 (7)	480 (8)	611 (13)	473 (7)	−30 (7)	−20 (9)	−142 (6)	521
	GI	22262 (2)	66313 (1)	46693 (2)	493 (2)	602 (2)	473 (2)	−13 (2)	−20 (2)	−142 (2)	523
	GII	22270 (4)	66312 (2)	46699 (4)	489 (6)	607 (6)	460 (6)	−5 (4)	−20 (4)	−142 (4)	519
	Mean	22264 (2)	66313 (1)	46694 (2)							

0·92 to 1·01 for Mo and from 0·99 to 1·06 for Ag. In spite of these strong variations Ext (222) = 1·0. This shows that, although for the two radiations on average the extinction correction seems satisfactory, the anisotropy is not yet described adequately by the second-order tensors for the size of the mosaic blocks and the mosaic spread. These model errors are expected to average out better for *GII* than for *GI*, since for *GII* a complete hemisphere of reflections is available for both Mo and Ag radiation. In agreement with this, *GI* deformation density maps turned out to be very irregular in comparison with *GII* deformation maps and will not be discussed further.

Calculation of deformation densities and potentials

Deformation densities

For both the *B* and *G* crystals *filtered* dynamic deformation densities have been computed according to

$$D_{\rm fi}(\mathbf{r}) = K\rho(\text{multi}; \mathbf{r}) - \rho(\text{IAM}; \mathbf{r}) \qquad (10)$$

with ρ(multi; **r**) the density corresponding to the multipole model, on a relative scale, and ρ(IAM; **r**) the density corresponding to a superposition of independent atoms (for *B* Mg^{2+} rather than Mg is taken). Coordinates and thermal parameters for the independent-atom model (IAM) are taken from the respective multipole refinements. Different types of scale factor have been applied for *G* and *B*:

(1) $K^G = K^G(\text{multi}) = \text{Pop}_p^{\rm sph}$ (free atom)/$\text{Pop}_p^{\rm sph}$ (multi) (equation 7). Equations (4*a*), (5), (7) and (10) give

$$D_{\rm fi}^G(\mathbf{r}) = K^G(\text{multi}) \sum_p \Delta\rho_p(\mathbf{r}_p). \qquad (11)$$

Relative errors $\Delta K/K$(multi) which are not compensated by model errors increase $D_{\rm fi}^G(\mathbf{r})$ by

$$\Delta D_{\rm fi}^G(\mathbf{r}) = [\Delta K^G/K^G(\text{multi})][\rho(\text{IAM}; \mathbf{r}) + D_{\rm fi}^G(\mathbf{r})]. \qquad (12)$$

Analysis of Si–O data deduced from quantum theoretical calculations with the present refinement method (van der Wal, 1982; van der Wal, Vos & Stewart, 1987) gave for a resolution comparable with the forsterite data a small scale error $\Delta K^G/K^G$ (multi) 0·04%. Moreover, in the present procedure errors in $\text{Pop}_p^{\rm sph}$ (multi) caused by correlation with extinction are, as far as the large ρ(IAM; **r**) term in (12) is concerned, balanced by errors in K(multi). If the influence of further systematic errors of the data set on K can be excluded, the errors at the atomic nuclei due to $\Delta K^G(\text{multi})/K^G$ are estimated to be smaller than 0·05 e Å^{-3}.

(2) $K^B = K^{HO} = 1{\cdot}01\,(1)K^B$ (multi). The use of K^{HO} rather than K^B (multi) increases $D^B_{fi}(\mathbf{r})$ with

$$\Delta D^B_{fi}(\mathbf{r}) = 0{\cdot}01[\rho(\text{IAM};\mathbf{r}) + D^B_{fi}(\mathbf{r})]. \qquad (13)$$

In view of the uncertainty in K^{HO} this increase is not significant.

Deformation potentials

The dynamic $\Delta\psi_{fi}(\mathbf{r})$ maps are computed with Fourier amplitudes $-4\pi[\Delta F_{fi}(\mathbf{H})/(\sin\theta/\lambda)^2]$, where $\Delta F_{fi}(\mathbf{H}) = KF_c(\mathbf{H};\text{multi}) - F_c(\mathbf{H};\text{IAM})$. This implies that errors in $\Delta\psi_{fi}(\mathbf{r})$ are primarily due to model errors which affect the low-order reflections. In contrast to $D^B_{fi}(\mathbf{r})$ the $\Delta\psi(\mathbf{r})$ for B contains Mg rather than Mg^{2+} as reference to keep the unit cell neutral.

Comparison of deformation densities for the SiO_4 tetrahedron

Sections of the $D^B_{fi}(\mathbf{r})$ and $D^G_{fi}(\mathbf{r})$ deformation densities are compared for O–Si–O planes in Fig. 2. For both B and G positive densities are observed at the Si–O bonds and in the oxygen lone-pair regions. Positions and heights of the maxima are notably different, however. In both cases the bond maxima are polarized towards O. Conflicting features are for instance: (1) Variation in height of bond maxima is smaller for G than for B. (2) For G, electrons in the lone-pair regions have a stronger tendency to be polarized towards Mg than for B. The polarization increases with decreasing O···Mg distances (Table 8), except when lone-pair electrons of the two O atoms of the same base-plane edge are polarized towards the same Mg ion. In this latter case polarization is relatively small. (3) For B the Si–O(−1) bond shows approximate rotational symmetry with the O(−1) lone-pair density concentrated around the Si–O(−1) line. These features, which would distinguish the Si–O(−1) bond from the other Si–O bonds, are masked in $D^G_{fi}(\mathbf{r})$ by the polarization of the lone-pair electrons discussed above. In view of the observed discrepancies between B and G no conclusions can be drawn concerning the influence of the surroundings on the Si–O bond deformation densities. Part of the discrepancies around the O atoms can be ascribed to the differences between the radial distribution functions for the O deformations in the two models (Table 4). If the Si–O $r_m \simeq 0{\cdot}4$ Å is taken as a reference, for B especially the oxygen octapole and hexadecapole deformations are too diffuse, whereas for G the oxygen dipole and quadrupole deformations are too sharp.

It is therefore reasonable to assume that at distances of 0·4 Å from O, oxygen deformations with $l \neq 0$ are described as much as possible by dipoles and quadrupoles in the B map and by octapoles in the G map.

Table 8. *Atomic distances* (Å) *and angles* (°)

The values are based on the mean coordinates of Table 7 and on the weighted average cell dimensions of Table 1. In this and in the following tables e.s.d.'s are given in parentheses in units of the last decimal places. The atom-numbering scheme refers to Fig. 1.

1. SiO_4 tetrahedron			
Si–O(−1)	1·6141 (2)		
Si–O(2)	1·6561 (1)		
Si–O(3)	1·6378 (1)		
O(−1)···O(2)	2·7469 (2)	O(−1)SiO(2)	114·27 (1)
O(−1)···O(3)	2·7591 (2)	O(−1)SiO(3)	116·08 (1)
O(2)···O(3)	2·5569 (1)	O(2)SiO(3)	101·84 (1)
O(3)···O(3^{ii})	2·5950 (2)	O(3)SiO(3^{ii})	104·79 (1)
2. $Mg(1)O_6$ octahedron			
Mg(1)···O(1)	2·0848 (1)		
Mg(1)···O(2)	2·0685 (1)		
Mg(1)···O(3)	2·1320 (1)		
O(1)···O(2)	2·8475 (2)	O(1)···O(3^{i})	3·1066 (1)
O(1)···O(3)	2·8518 (2)	O(2)···O(3)	2·5569 (2)
O(1)···O(2^{i})	3·0236 (1)	O(2)···O(3^{i})	3·3331 (2)
3. $Mg(2)O_6$ octahedron			
Mg(2)···O(1)	2·1779 (1)	Mg(2)···O(3)	2·2105 (1)
Mg(2)···O(2^{iii})	2·0470 (1)	Mg(2)···O(3^{iv})	2·0670 (1)
O(2^{iii})···O(3^{iv})	2·9313 (2)	O(1)···O(3)	2·8518 (2)
O(3)···O(3^{ii})	2·5950 (2)	O(1)···O(3^{iv})	3·0211 (1)
O(3)···O(3^{v})	2·9913 (1)	O(2^{iii})···O(3)	3·1834 (1)
O(3^{iv})···O(3^{v})	3·3860 (2)		
4. Coordination of O(1) by Mg and Si			
O(1)···Si(+1)	1·6141 (1)		
O(1)···Mg(1)	2·0848 (1)		
O(1)···Mg(2)	2·1779 (1)		
Si(+1)O(1)Mg(1)	122.76 (1)	Mg(1)O(1)Mg(1^{ii})	91·65 (1)
Si(+1)O(1)Mg(2)	118·63 (1)	Mg(1)O(1)Mg(2)	97·25 (1)
5. Coordination of O(2) by Si and Mg			
O(2)···Si	1·6561 (1)		
O(2)···Mg(1)	2·0685 (1)		
O(2)···Mg(2^{iii})	2·0470 (1)		
SiO(2)Mg(1)	92·06 (1)	Mg(1)O(2)Mg(1^{ii})	92·59 (1)
SiO(2)Mg(2^{iii})	122·52 (1)	Mg(1)O(2)Mg(2^{iii})	124·23 (1)
6. Coordination of O(3) by Si and Mg			
O(3)···Si	1·6378 (1)	O(3)···Mg(2)	2·2105 (1)
O(3)···Mg(1)	2·1320 (1)	O(3)···Mg(2^{v})	2·0670 (1)
SiO(3)Mg(1)	90·33 (1)	Mg(1)O(3)Mg(2)	94·89 (1)
SiO(3)Mg(2)	95·59 (1)	Mg(1)O(3)Mg(2^{v})	117·26 (1)
SiO(3)Mg(2^{v})	124·17 (1)	Mg(2)O(3)Mg(2^{v})	128·98 (1)

Deformation properties at the Mg cations

Deformation densities and potentials

Fig. 3 shows $D^B_{fi}(\mathbf{r})$ and $D^G_{fi}(\mathbf{r})$ sections for planes containing the Mg atoms. For both B and G the dynamic $D_{fi}(\mathbf{r})$ density at Mg(2) lies close to zero, and Mg(2) is approached by positive and negative density areas. For Mg(1) the situation is different for the two cases. For B Mg(1) lies in a positive density area, whereas for G all around Mg(1) and especially along Mg(1)···Si the deformation density is negative. This conflicting result is bound to give contradictory values for

$$\Delta[\Delta\psi] = \Delta\psi(\text{Mg1}) - \Delta\psi(\text{Mg2}) \qquad (14)$$

describing the difference between the deformation potentials at Mg(1) and Mg(2). The calculated values, $\Delta[\Delta\psi]^B = -0{\cdot}36$ and $\Delta[\Delta\psi]^G = +0{\cdot}48$ e Å^{-1}, are roughly equal in magnitude, but opposite in sign.

Conclusions concerning electrostatic potential differences in the voids can thus not be drawn.

Electric field gradients

In Table 9 experimental data on the electric field gradients (EFG) at the Mg-cation sites obtained by NMR techniques and X-ray diffraction are compared. The NMR values were measured on ^{25}Mg in forsterite by Derighetti, Hafner, Marxer & Rager (1978). The sign of V_{zz} could not be determined. The values for B and GII are obtained by direct-space calculations according to Stewart (1979) from the static quadrupole moment of the Mg atom under consideration. Their mean value is given by 'Mean'. According to Rager & Schmidt (1981) (RS), V_{zz} (total) can be divided into three parts [RS formulae (2) and (13)]:

$$V_{zz}\,(\text{total}) \simeq V_{zz}\,(\text{overlap}) + V_{zz}\,(\text{external}) + V_{zz}\,(\text{internal}) \qquad (15)$$

with $V_{zz}\,(\text{int}) = -\gamma^{\infty}_{Mg} V_{zz}\,(\text{ext})$, where γ^{∞}_{Mg} is the Sternheimer antishielding factor. In (15) it is assumed that

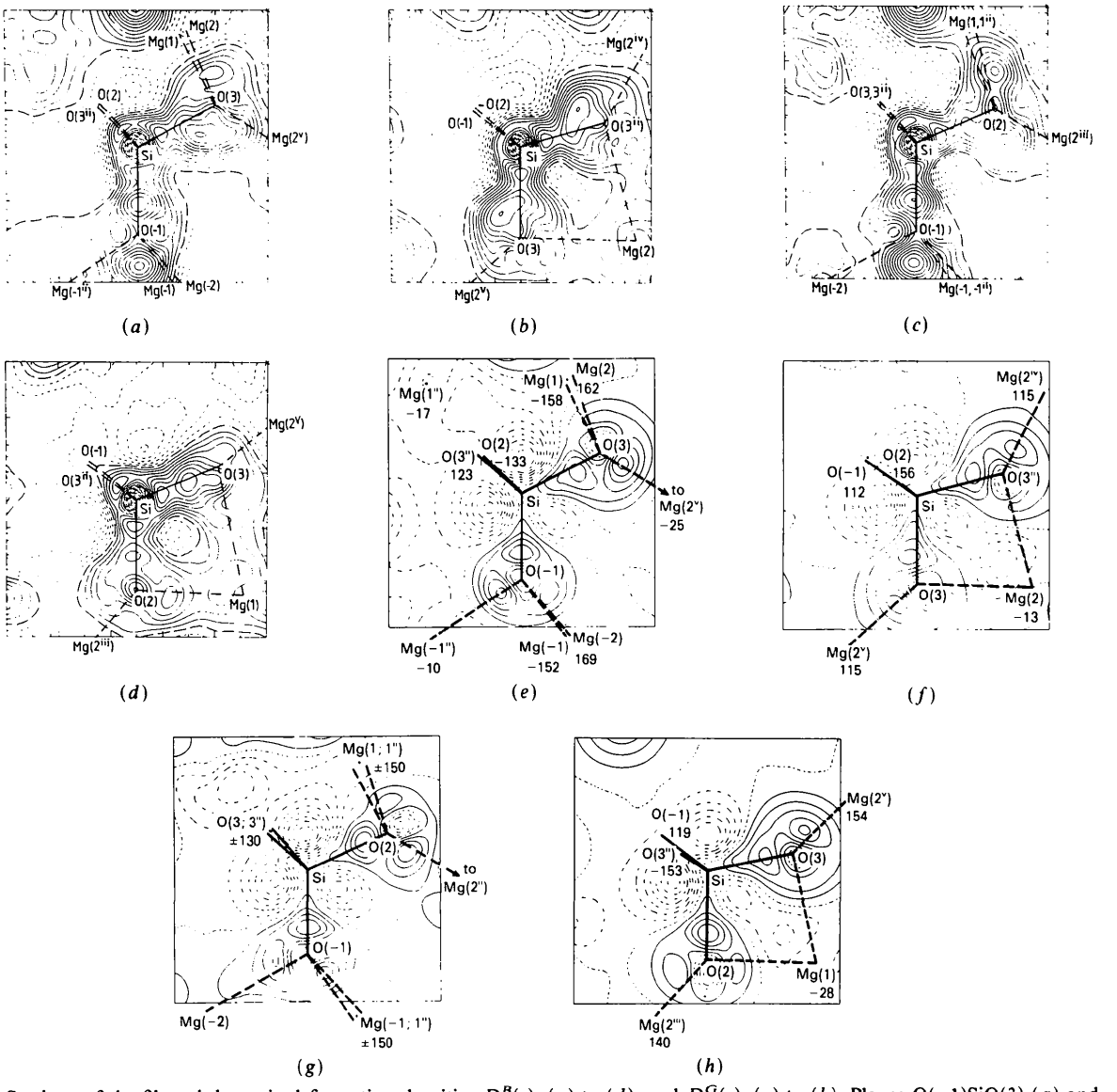

Fig. 2. Sections of the filtered dynamic deformation densities $D^{B}_{fi}(\mathbf{r})$, (*a*) to (*d*), and $D^{G}_{fi}(\mathbf{r})$, (*e*) to (*h*). Planes O(−1)SiO(3) (*a*) and (*e*), O(3)SiO(3ii) (*b*) and (*f*), O(−1)SiO(2) (*c*) and (*g*), and O(2)SiO(3) (*d*) and (*h*). Contours in these and in all following $D_{fi}(\mathbf{r})$ maps at intervals of 0·05 e Å^{-3}. For $D^{B}_{fi}(r)$ positive contours full lines, negative lines dotted and zero contours dashed. All $D^{B}_{fi}(\mathbf{r})$ maps are artificially increased by 0·055 e Å^{-3}, because no correction has been made for the occurrence of Mg^{2+} rather than Mg in the IAM for *B*. For $D^{G}_{fi}(\mathbf{r})$ positive contours full lines, negative contours dashed and zero contours dotted. Distances of atoms from the plane of the section are indicated in (*e*) to (*h*) in units of 10^{-2} Å.

the main axes of V_{zz} (ext) and V_{zz} (int) coincide. The X-ray values for V_{zz} should be compared with V_{zz} (int), as the internal EFG part is due to the charge distribution in the atom containing the nucleus considered. With $\gamma^{\infty}_{Mg} = -3{\cdot}5$ and the RS overlap values V_{zz} (overlap Mg1) $= -0{\cdot}082$ and V_{zz} (overlap Mg2) $= 0{\cdot}241$ Å^{-3} (RS p. 173) we obtain (in e Å^{-3}):

$$\text{Mg(1)}: V_{zz}^{\text{NMR}}(\text{int}) = 0{\cdot}57 \quad \text{for } V_{zz}+;$$
$$V_{zz}^{\text{NMR}}(\text{int}) = -0{\cdot}44 \quad \text{for } V_{zz}-$$
$$\text{Mg(2)}: V_{zz}^{\text{NMR}}(\text{int}) = 0{\cdot}25 \quad \text{for } V_{zz}+;$$
$$V_{zz}^{\text{NMR}}(\text{int}) = -0{\cdot}44 \quad \text{for } V_{zz}-.$$

The X-ray values show good agreement with V_{zz}^{NMR} (int), if for Mg(1) V_{zz} is taken negative, and for Mg(2) V_{zz} is taken positive. The X-ray and NMR directions of the principal axes of the EFG tensor agree as well as one can expect in view of the assumptions made above, and the fact that none of the X-ray quadrupole populations is larger than 4·5 times its standard deviation. The RS extended charge model has given positive calculated V_{zz} signs for both Mg(1) and Mg(2), although calculated and NMR-observed components of the EFG tensor agree better for Mg(2) than for Mg(1). Sign reversal of the X-ray values for Mg(1) changes B by 4σ and GII by 3σ, and is thus not very probable. However, in view of the differences between the B and GII deformation potentials the conclusions drawn from the X-ray work should not be considered as final.

Concluding remarks

In view of the strong extinction corrections, corresponding positional and thermal parameters of B and

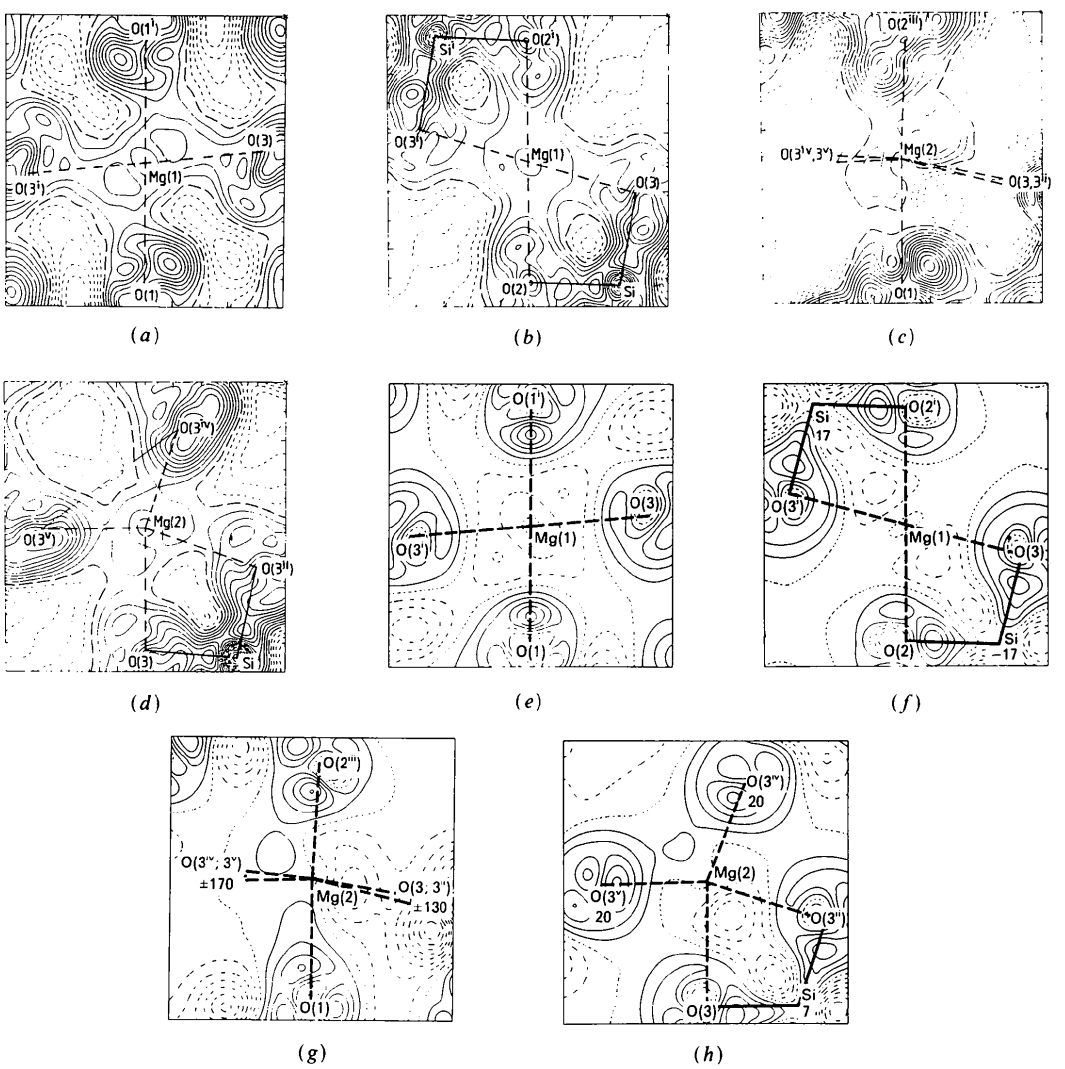

Fig. 3. Sections of the filtered dynamic deformation densities $D_{fi}^{B}(\mathbf{r})$, (*a*) to (*d*), and $D_{fi}^{G}(\mathbf{r})$, (*e*) to (*h*). Planes O(1)Mg(1)O(3), (*a*) and (*e*), O(2)Mg(1)O(3), (*b*) and (*f*), O(1)Mg(2)O(2^{iii}), (*c*) and (*g*), and O(3)Mg(2)O(3^{ii}), (*d*) and (*h*). For further details see Fig. 2.

Table 9. *Electric field gradients (EFG) at the* Mg *atoms*

aX–cZ: direction cosines of main tensor axes *X*, *Y*, *Z* with crystal axes **a**, **b**, **c**. *Δ*: angle between corresponding main axes from X-ray and NMR. *η*: asymmetry parameter. $|V_{zz}|$: absolute value of EFG along *Z* from quadrupole coupling constant (sign unknown). V_{zz}: EFG along *Z* including sign. For Mg(2) one of the axes lies along **c** because of the mirror symmetry.

	aX	*bX*	*cX*	(*Δ*°)	*aY*	*bY*	*cY*	(*Δ*°)	*aZ*	*bZ*	*cZ*	(*Δ*°)	*η*	$\|V_{zz}\|$	V_{zz}
Mg(1) at 0,0,0															
NMR	0·602	−0·574	−0·559		−0·743	−0·139	−0·656		0·309	0·809	−0·500		0·963 (3)	0·652	
B	0·543	−0·792	−0·278	20	−0·825	−0·440	−0·355	25	0·159	0·423	−0·892	33	0·43		−0·42 (21)
*G*II	0·848	0·139	−0·515	44	−0·454	−0·326	−0·838	21	−0·276	0·940	−0·208	39	1·42		−0·52 (35)
Mean	0·804	−0·378	−0·458	17	−0·670	−0·401	−0·625	16	−0·068	0·778	−0·624	23	0·93		−0·47
Mg(2) at 0·9916, 0·2774, 0·25															
NMR	0·319	0·948	0		0	0	1		0·948	−0·319	0		0·396 (2)	0·563	
B	0·155	0·988		10					0·988	−0·155		10	0·79		0·11 (13)
*G*II	0·629	0·777		20					0·777	−0·629		20	0·24		0·37 (22)
Mean	0·407	0·914		5					0·914	−0·407		5	0·52		0·24

Quadrupole populations. Populations for *B* and *G* are very different since the *α* values [for *B*: refined $\alpha(l=2;\ \mathrm{Mg1}) = 1{\cdot}46$, $(l=2;\ \mathrm{Mg2}) = 2{\cdot}33$, for *G*II $\alpha(l=2)$ fixed at 3·0] give different normalization constants in (5*a*); $n(B) = n(G\mathrm{II}) = 4$.

			$q_x^2 - q_y^2$	q_xq_y	q_xq_z	q_yq_z	$q_z^2 - \frac{1}{3}$
B	Mg(1)	Pop	−54 (23)	228 (51)	37 (55)	155 (58)	−80 (38)
	Mg(2)	Pop	−5·6 (14)	6·1 (33)			−13·5 (28)
*G*II	Mg(1)	Pop	−1·0 (12)	−3·6 (27)	−3·7 (23)	−5·3 (33)	−3·6 (25)
	Mg(2)	Pop	−1·5 (13)	4·3 (25)			0·6 (25)

G show a remarkably good agreement. Difficulties occur with the deformation properties, however, when extinction is present. With our present knowledge of the extinction phenomenon filtered deformation properties have to be extracted from the data which requires use of a refinement model. The present study shows that problems are encountered with the radial distribution functions of the deformations. If, with use of SEF's, *α*'s are refined (as in *B*); the deformations tend to become too diffuse, and deformations with incorrect radial distributions may not show up properly. Constraint of *α*, on the other hand (as in *G*), requires *a priori* knowledge of the radial distribution. It is hard to detect whether the guesses made for the various radial distribution functions are correct, and whether due to incorrect guesses deformations are suppressed. The tendency of deformation functions to become too diffuse, when refined as in *B*, indicates that the multipole refinement tends to yield parameters which, especially in the low-order region, mask inadequately corrected systematic errors in the $F_o(\mathbf{H})$ values. This has the serious implication that deformation densities filtered from $F_o(\mathbf{H})$ values affected by extinction and/or other systematic errors are not unique, but influenced by the chosen correction formalism(s) and the set-up of the multipole refinement. For forsterite the *B* and *G* deformation properties look acceptable by themselves, but are notably different, and neither of them may come as close to the truth as desirable. It must thus be concluded that not too much value should be attached to deformation properties deduced from X-ray diffraction intensities which are considerably affected by extinction. The present authors will not pursue the research on forsterite. The data sets are available on request at the Electron Density Data Bank quoted in the *Abstract*.

Preparation of and measurements on the *G*I crystal and determination of the cell constants in Groningen were carried out by Dr J. L. de Boer. The investigations were supported, in part, by the Netherlands Foundation for Chemical Research (SON) with financial aid from the Netherlands Organization for the Advancement of Pure Research (ZWO) (RJvdW and AV), by the Deutsche Forschungsgemeinschaft (AK) and, in part, by NSF grant CHE-80-16165. One of us (AK) is indebted to the Carnegie-Mellon University, Pittsburgh, PA, for financial support during his stay at the Department of Chemistry. Many fruitful discussions with R. F. Stewart and M. A. Spackman, both in Pittsburgh and in Groningen, are gratefully acknowledged. The computations for the *G* crystals were carried out on a Cyber 170/760 at the Computing Centre of the University of Groningen, computations for *B* were performed at the Computing Centre of the University of Bonn (IBM) and at the Department of Chemistry of the Carnegie-Mellon University, Pittsburgh (VAX). Finally, the authors wish to thank the referees and the editor for their useful comments.

References

BECKER, P. J. & COPPENS, P. (1974). *Acta Cryst.* **A30**, 129–147, 148–153.

BECKER, P. J. & COPPENS, P. (1975). *Acta Cryst.* **A31**, 417–425.

BENTLEY, J. J. & STEWART, R. F. (1976). *Acta Cryst.* **A32**, 910–914.

BIRLE, J. D., GIBBS, G. V., MOORE, P. B. & SMITH, J. V. (1968). *Am. Mineral.* **53**, 807–824.

CLEMENTI, E. (1965). *Tables of Atomic Functions.* San Jose Research Laboratory, IBM Corporation, San Jose, California, USA.

CROMER, D. T. & LIBERMAN, D. (1970). *J. Chem. Phys.* **53**, 1891–1898.

DERIGHETTI, B., HAFNER, S., MARXER, H. & RAGER, H. (1978). *Phys. Lett. A*, **66**(2), 150–152.

HAMILTON, W. C., ROLLETT, J. S. & SPARKS, R. A. (1965). *Acta Cryst.* **18**, 129-130.
HEHRE, W. J., STEWART, R. F. & POPLE, J. A. (1969). *J. Chem. Phys.* **51**, 2657-2664.
HELMHOLDT, R. B. & VOS, A. (1977). *Acta Cryst.* A**33**, 456-465.
International Tables for X-ray Crystallography (1972). Vol. II, p. 299. Birmingham: Kynoch Press. (Present distributor D. Reidel, Dordrecht.)
KIRFEL, A., WILL, G. & STEWART, R. F. (1983). *Acta Cryst.* B**39**, 175-185.
MCLEAN, A. D. & YOSHIMINE, M. (1967). *Tables of Linear Molecule Wave Functions. IBM J. Res. Dev.* **12**, Suppl. 74.
NELMES, R. J. (1980). *Acta Cryst.* A**36**, 641-653.
RAGER, H. & SCHMIDT, P. C. (1981). *Phys. Chem. Miner.* **7**, 169-176.
STEWART, R. F. (1976). *Acta Cryst.* A**32**, 565-574.
STEWART, R. F. (1979). *Chem. Phys. Lett.* **65**, 335-342.
STEWART, R. F. (1985). Personal communication.
STEWART, R. F., BENTLEY, J. J. & GOODMAN, B. (1975). *J. Chem. Phys.* **63**, 3786-3793.
STEWART, R. F. & SPACKMAN, M. A. (1981). *VALRAY Users Manual.* Preliminary Draft, Department of Chemistry, Carnegie-Mellon Univ., Pittsburgh, PA 15213, USA.
WAL, H. R. VAN DER, DE BOER, J. L. & VOS, A. (1979). *Acta Cryst.* A**35**, 685-688.
WAL, H. R. VAN DER & VOS, A. (1979). *Acta Cryst.* B**35**, 1793-1804.
WAL, R. J. VAN DER (1982). Thesis, Univ. of Groningen.
WAL, R. J. VAN DER, VOS, A. & STEWART, R. F. (1987). In preparation.
WILSON, A. J. C. (1976). *Acta Cryst.* A**32**, 781-783.

Acta Cryst. (1987). B**43**, 143-146

Structure of Na_2SO_4(I) at 693 K

BY H. NARUSE, K. TANAKA, H. MORIKAWA AND F. MARUMO

Research Laboratory of Engineering Materials, Tokyo Institute of Technology, Nagatsuta 4259, *Midori, Yokohama* 227, *Japan*

AND B. N. MEHROTRA

Department of Bio-Physics, All India Institute of Medical Science, New Delhi 110029, *India*

(*Received* 27 *February* 1986; *accepted* 22 *September* 1986)

Abstract

The crystal structure of Na_2SO_4(I) at 693 K was investigated by X-ray diffraction and refined to an R value of 0·049 for 63 observed independent reflections. Na_2SO_4(I) has the space group $P6_3/mmc$ with $a = 5{\cdot}444\ (2)$, $c = 7{\cdot}347\ (6)$ Å, $V = 188{\cdot}6(2)$ Å^3 and $Z = 2$. $M_r = 142{\cdot}04$, $D_x = 2{\cdot}501$ Mg m^{-3}, $F(000) = 140$ and μ(Mo $K\alpha$) = 0·9466 mm^{-1}. The SO_4 tetrahedron mainly adopts the apex model orientation with one of the apices pointing statistically up and down the c axis. Further, the apical O atom is not exactly on the threefold axis passing through the central S atom, but deviates slightly from it. A small fraction of SO_4 groups take the orientation of the edge model at 693 K.

Introduction

Five modifications designated as phases (I) to (V) have been reported for Na_2SO_4 crystals to date (Kracek & Gibson, 1930; Kracek & Ksanda, 1930; Saito, Kobayashi & Maruyama, 1982; Eysel, Höfer, Keester & Hahn, 1985). Among these modifications, Na_2SO_4(IV) is supposed to be metastable and the phase relation has not yet been well established. Precise structure determinations of the room-temperature phase Na_2SO_4(V) and of the intermediate phase Na_2SO_4(III) were carried out by Nord (1973) and Mehrotra (1981), respectively. Since the stable temperature range of Na_2SO_4(II) is narrow, the structural details of Na_2SO_4(II) are unknown. Several structure models have been proposed for the high-temperature phase Na_2SO_4(I). The arrangement of Na^+ and SO_4^{2-} ions is the same in all these models except for the orientation of SO_4^{2-} groups.

Recently, Eysel *et al.* (1985) carried out a detailed structure investigation of yttrium-stabilized Na_2SO_4(I) at room temperature, and revealed that the structure agrees well with the model proposed by Höfer (1979), where one of tetrahedral edges of the SO_4^{2-} group is parallel to the c axis of the hexagonal lattice and statistically the anion takes three crystallographically equivalent orientations in equal probability around the threefold rotation axis. However, the mode of the statistical distribution may change with temperature as pointed out by Eysel *et al.* (1985). Therefore, it is of interest to obtain the structural details of Na_2SO_4(I) at high temperatures where the modification is stable.

Amirthalingam, Karkhanavala & Rao (1977) reported that crystals of Na_2SO_4(III), which show topotactic transformation to Na_2SO_4(I), remain

0108-7681/87/020143-04$01.50